

## Geometric entanglement of a photon and spin qubits in diamond

Yuhei Sekiguchi<sup>1</sup>, Yuki Yasui<sup>2</sup>, Kazuya Tsurumoto<sup>2</sup>, Yuta Koga<sup>2</sup>, Raustin Reyes<sup>2</sup> & Hideo Kosaka<sup>1,2</sup><sup>✉</sup>

Geometric nature, which appears in photon polarization, also appears in spin polarization under a zero magnetic field. These two polarized quanta, one travelling in vacuum and the other staying in matter, behave the same as geometric quantum bits or qubits, which are promising for noise resilience compared to the commonly used dynamic qubits. Here we show that geometric photon and spin qubits are entangled upon spontaneous emission with the help of the spin – orbit entanglement inherent in a nitrogen-vacancy center in diamond. The geometric spin qubit is defined in a degenerate subsystem of spin triplet electrons and manipulated with a polarized microwave. An experiment shows an entanglement state fidelity of 86.8%. The demonstrated entangled emission, combined with previously demonstrated entangled absorption, generates purely geometric entanglement between remote matters in a process that is insensitive of time, frequency, and space mode matching, which paves the way for building a noise-resilient quantum repeater network or a quantum internet.

<sup>1</sup>Institute of Advanced Sciences, Yokohama National University, 79-5 Tokiwadai, Hodogaya, Yokohama 240-8501, Japan. <sup>2</sup>Department of Physics, Graduate School of Engineering Science, Yokohama National University, 79-5 Tokiwadai, Hodogaya, Yokohama 240-8501, Japan. ✉email: [kosaka-hideo-yp@ynu.ac.jp](mailto:kosaka-hideo-yp@ynu.ac.jp)

Quantum entanglement between remote qubits is an essential element for not only quantum networks<sup>1–3</sup> but also quantum computers as well as quantum metrology. In these technologies, a quantum medium (degrees of freedom or material) that carries quantum information must be converted or interfaced between functional elements, such as registers, memories, and transmission qubits, just as in classical information technology. A hybrid quantum system is thus attractive as a quantum interface<sup>4</sup>. A candidate for such a hybrid quantum system is a color center in diamond<sup>5</sup>, such as nitrogen-vacancy (NV)<sup>6–8</sup>, silicon-vacancy (SiV)<sup>9,10</sup>, germanium-vacancy (GeV)<sup>11–13</sup>, and tin-vacancy (SnV)<sup>14–16</sup> centers, which provides spin memories accessible by light<sup>17–20</sup> and enables entanglement generation between a photon and a spin<sup>21–25</sup>. An electron spin in those color centers, surrounded by a number of carbon isotope spins, is commonly manipulated under a strong magnetic field<sup>26–31</sup>, which hinders the quantum medium conversion. For example, superconducting qubits, which are promising for quantum computing<sup>32</sup>, work under a weak magnetic field to avoid superconducting breakdown. A zero magnetic field is further desired to achieve high homogeneity in scaling up the system.

Geometric spin manipulation under a zero magnetic field<sup>33–37</sup> has been demonstrated by utilizing the degenerate subspace of the spin-triplet state of a negatively charged NV center with a polarized microwave<sup>38–40</sup> or with a polarized light<sup>41,42</sup>. Quantum state transfer from a photon polarization into a nuclear spin near an NV center<sup>43,44</sup> has also been demonstrated based on entangled absorption<sup>45</sup>. In this work, we demonstrate entanglement generation between spin and photon polarizations with spontaneous

emission under a zero magnetic field, which will enable the spontaneous generation of entanglement between remote spins when combined with the quantum state transfer (Fig. 1a).

## Results

**System and scheme.** A negatively charged NV center has a spin-triplet electronic structure. In the orbital ground state, it forms a V-shaped spin-1 three-level structure with degenerate  $|m_S = \pm 1\rangle_S$  states and a zero-field split  $|m_S = 0\rangle_S$  state due to spin–spin interaction. These states are coupled with the degrees of freedom of the microwave polarization, resulting in transitions selective to the right- and left-circular microwave polarization. Similarly, the degenerate  $|\pm 1\rangle_S$  states and one of the excited states  $|A_2\rangle$ , which is split from other excited states by the spin–orbit and spin–spin interactions, constitute a  $\Lambda$ -shaped three-level structure, resulting in transitions selective to left- and right-circular light polarization, respectively<sup>46</sup> (Fig. 1b, c). Therefore, the degenerate spin subspace, called a geometric spin qubit, is accessible with an arbitrarily polarized light or microwave. Universal holonomic quantum gates<sup>47</sup> are defined on the geometric spin qubit with a geometric phase given via a cyclic transition between the qubit space and ancillary state  $|0\rangle_S$  or  $|A_2\rangle$ <sup>40,41</sup>. The correlation between the spin and photon polarizations also exists in the process of absorbing and emitting a single photon: when the state prepared at  $|A_2\rangle$  relaxes by emitting a photon with the polarization entangled with the spin polarization. In contrast, when a photon is absorbed to excite the electron orbital into the  $|A_2\rangle$  state, the photon polarization needs to be correlated with the spin polarization<sup>45</sup>, thus enabling the Bell state measurement conditioned on the absorption event.

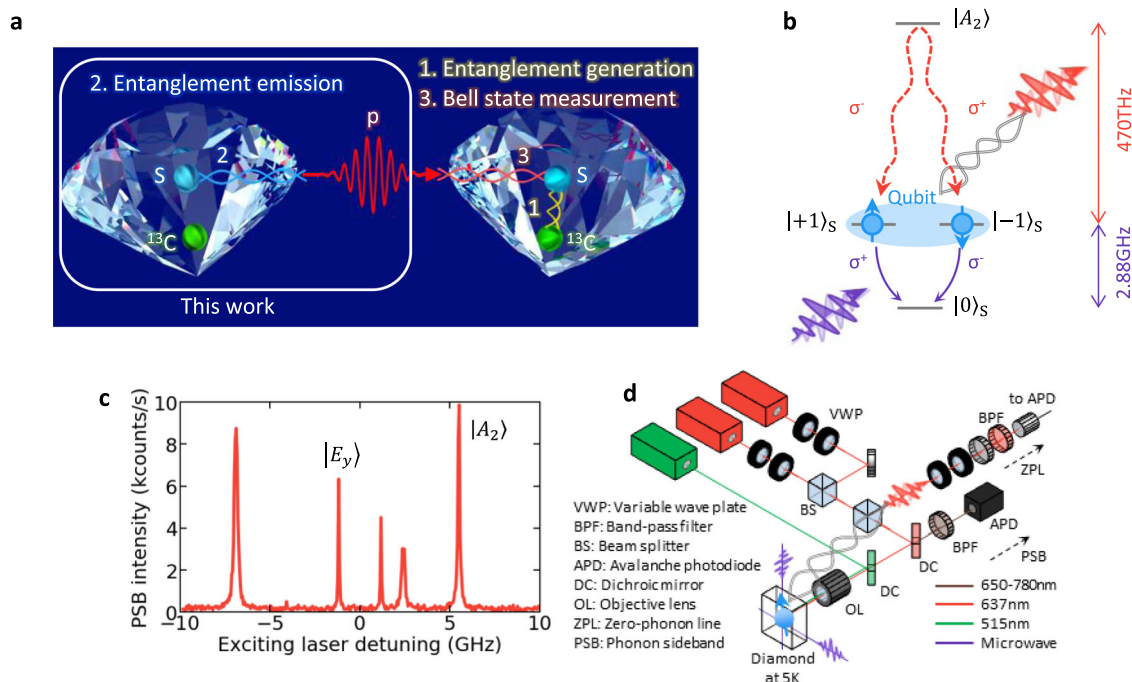


**Fig. 1 Geometric entanglement of diamond NV center.** **a** The supposed protocol of the one-way quantum repeater system with an NV center at each node. A photon is emitted from one node (left), leaving an electron entangled with the emitted photon. The success of the photon storage in the other node (right) establishes the entanglement between two adjacent nodes. **b** Rhombic four-level structure under a zero magnetic field. The degenerate  $|\pm 1\rangle_S$  states are the basis of the geometric spin qubit. One of the excited states  $|A_2\rangle$  and the ground state  $|0\rangle_S$  are regarded as ancillary states, which are used to access the geometric spin qubit by the polarization of light and microwave fields. The spontaneous emission from  $|A_2\rangle$  generates the entanglement between the polarizations of the photon and the geometric spin qubit.  $\sigma^+$  and  $\sigma^-$  represent right- and left-circular polarizations. **c** Photoluminescence excitation (PLE) spectrum. **d** Experimental optical setup. The green laser initializes the charge and the spin state of the NV center. The red laser is used for excitation to  $|A_2\rangle$  and the spin measurement of  $|0\rangle_S$ . The polarization of ZPL emission from  $|A_2\rangle$  is arbitrarily projected by a variable wavelength plate and a polarizer, and then coupled to a single-mode fiber to be measured by APD. On the other hand, the phonon sideband (PSB) emission from  $|E_y\rangle$  for spin measurement is extracted by a band-pass filter and measured by APD.

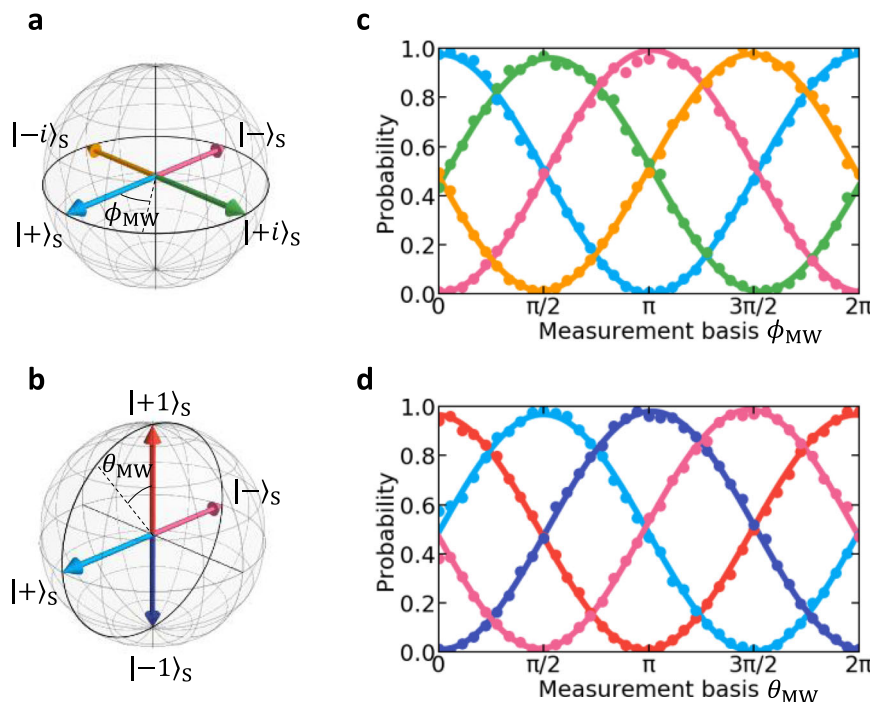


**Fig. 2 Operation of geometric qubit.** **a, c** Two-dimensional tomography in the xy-plane of the prepared geometric spin qubit states  $|+\rangle_s$ ,  $|+i\rangle_s$ ,  $|-\rangle_s$ , and  $|-i\rangle_s$ . **b, d** Two-dimensional tomography in the xz-plane of the prepared geometric spin qubit states  $|+1\rangle_s$ ,  $|+\rangle_s$ ,  $|-\rangle_s$ , and  $|-\rangle_s$ . Bloch vectors indicate prepared geometric spin qubit states. Standard deviation is smaller than the size of the dots.

**Geometric operation.** A microwave  $\pi$ -pulse consisting of an arbitrary polarization state  $|\psi\rangle_{MW} = \cos\theta_{MW}|+1\rangle_{MW} + e^{-i\phi_{MW}}\sin\theta_{MW}|-1\rangle_{MW}$  excites a geometric spin qubit state  $|\psi\rangle_s = \cos\theta_{MW}|+1\rangle_s + e^{-i\phi_{MW}}\sin\theta_{MW}|-1\rangle_s$  from the ground ancilla state  $|0\rangle_s$ . Here,  $\theta_{MW}$  and  $\phi_{MW}$  respectively denote the polar and azimuthal angles in the Poincaré sphere based on the right- and left-circular polarization states,  $|+1\rangle_{MW}$  and  $|-1\rangle_{MW}$ . In reverse, the microwave  $\pi$  pulse rotates the arbitrary qubit state to  $|0\rangle_s$ ; the state rotated to  $|0\rangle_s$  can be read out by spin-dependent excitation to  $|E_y\rangle$ . We first evaluate the intensity and polarization of microwaves applied from two wires (Fig. 1d) to determine the parameters of the microwave voltage and phase that generate the arbitrary microwave polarization<sup>40</sup>. We then generate modulated waveforms with the GRAPE algorithm<sup>48</sup> to increase the manipulation fidelity within the limited Rabi frequency, 2.5 MHz (see Supplementary Note 1). Any geometric spin qubit states are prepared and read out with the corresponding microwave polarization (Fig. 2a, b). Figure 2c, d show two-dimensional tomography on six prepared states  $\{|+\rangle_s = (|+1\rangle_s + |-1\rangle_s)/\sqrt{2}, |-\rangle_s = (|+1\rangle_s - |-1\rangle_s)/\sqrt{2}, |i\rangle_s = (|+1\rangle_s + i|-1\rangle_s)/\sqrt{2}, |-i\rangle_s = (|+1\rangle_s - i|-1\rangle_s)/\sqrt{2}, |+1\rangle_s, |-1\rangle_s\}$ . The resulting average fidelity including the state preparation and measurement is 97% (Fig. 2) (see Supplementary Note 2).

**Spin-photon entanglement.** To observe the photon emission process from  $|A_2\rangle$  to the ground state, we measure the zero-phonon line (ZPL) emission after resonant excitation. Since the wavelengths of the excitation light and the emitted photon are the same, it is necessary to separate the excitation light reflected at the optical element and the diamond surface from the emitted photon in space and time. In the present setup, although the reflected light is temporally eliminated by a two-stage electro-optic modulator (EOM), the overall extinction ratio is not sufficient. Therefore, we make the polarization of the excitation light

orthogonal to the polarization of the photon measurement. Note that the polarization of the excitation light does not affect the measurement results because the excitation is only for preparing the quantum state to  $|A_2\rangle$ . For practical use, since the polarizer cannot be used to eliminate the excitation light, either an AR coating of the diamond surface, a more elaborate optical design, or an improvement of the extinction ratio of the optical modulator is needed. Another possible way to eliminate the excitation light is nonresonant excitation with a wavelength filter to extract only the  $|A_2\rangle$  photon.

Figure 3a shows the ZPL emission intensity depending on the avalanche photodiode (APD) gate delay time, where the gate width is fixed at 10 ns. Since the probabilities of detecting a photon and a spin in the present setup are  $3 \times 10^{-6}$  and 0.15, respectively, simultaneous detection rarely occurs. We thus measure the spin state conditioned on the photon detection (Fig. 3b). Since the reflected excitation light is slightly included in the detected photons, as shown in Fig. 3a, the completely mixed spin state is probabilistically measured. In Fig. 3c, the estimated error detection count is subtracted to show only the intrinsic entangled state. The obtained results are in good agreement with the entangled state written as  $|\Psi_+\rangle = \frac{|+1\rangle_p|-1\rangle_s + |-1\rangle_p|+1\rangle_s}{\sqrt{2}} = \frac{|+1\rangle_p|+1\rangle_s - |-1\rangle_p|-1\rangle_s}{\sqrt{2}} = \frac{-i|+1\rangle_p|+1\rangle_s + i|-1\rangle_p|-1\rangle_s}{\sqrt{2}}$ , which indicates odd, even, and even parity along with the z-, x-, and y-axis measurements, where  $|+1\rangle_p$  and  $|-1\rangle_p$  denotes right- and left-circular polarization of the optical photon. The estimated state fidelity is 86.8%, which is limited mainly by NV-axis misalignment (6%), spin phase rotation (2%), spin measurement error (2%), and hybridization of excited states due to non-axial strain (1%) (Fig. 3d) (see Supplementary Note 3). The axis misalignment can be corrected by balancing the optical or spin systems since it is a coherent error (discussed later). The spin phase rotation is attributed mainly to the residual magnetic field and hyperfine interaction between electrons and the nitrogen nuclear spin during the

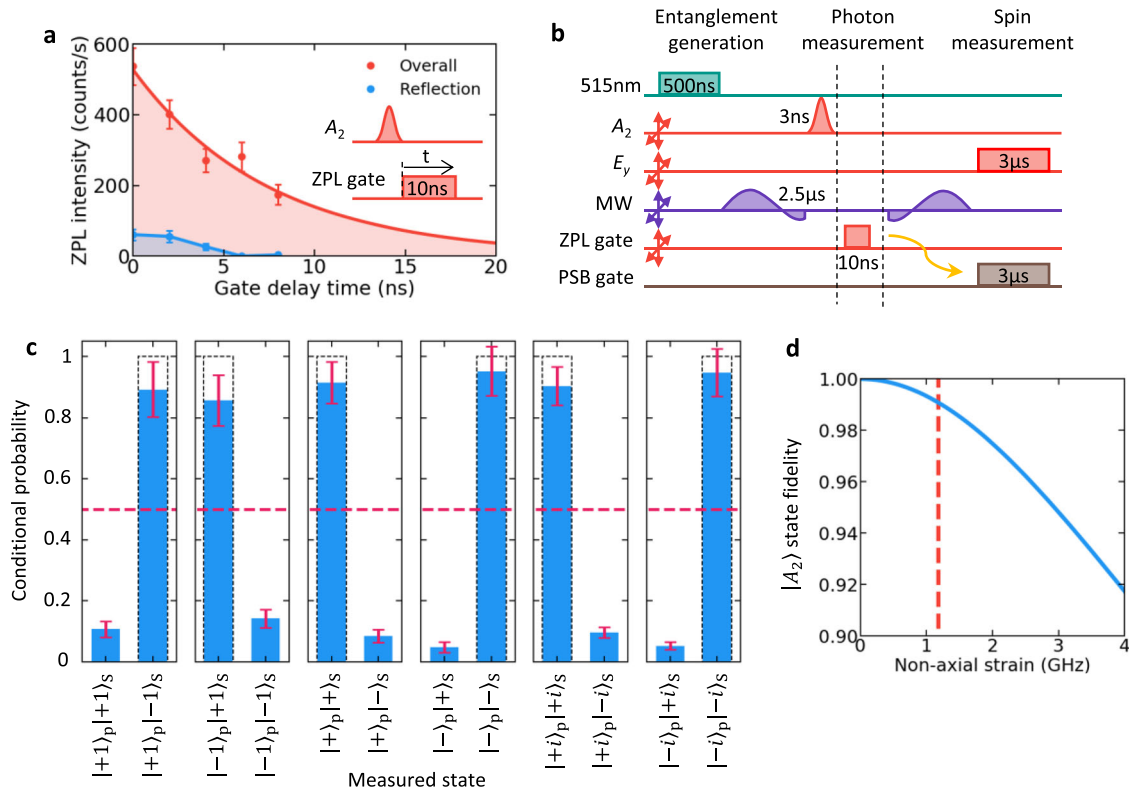


**Fig. 3 Measurement of spin-photon polarization correlations.** **a** Time dependence of the ZPL emission from  $|A_2\rangle$ . Although the measured polarization of the emitted photon is orthogonal to the excitation light, there is still a background (blue line) due to reflection. **b** Experimental sequence of the measurement of entangled emission. The spin state is measured with the microwave polarization after the detection of the polarized photon. **c** Spin state probability conditioned on the photon polarization. Blue bars are experimental data. 117, 130, 201, 147, 237, and 167 events were measured for  $|+1\rangle_p | -1\rangle_s$ ,  $|+1\rangle_p | +1\rangle_s$ ,  $| -1\rangle_p | +1\rangle_s$ ,  $| -1\rangle_p | -1\rangle_s$ ,  $|+i\rangle_p | +i\rangle_s$ , and  $| -i\rangle_p | -i\rangle_s$ , respectively. Dotted lines indicate the ideal probabilities for the maximally entangled state. **d** Strain dependence of the state fidelity of the  $|A_2\rangle$  state, simulated from the Hamiltonian based on ref. <sup>6</sup>. The fidelity is calculated by  $\text{tr}(\rho_{\text{ideal}} \rho_{\text{sim}})$ , where  $\rho_{\text{ideal}}$  and  $\rho_{\text{sim}}$  denote density matrix of ideal and simulated  $|A_2\rangle$  states. Red dotted line indicates the magnitude of the non-axial strain of the NV center used in the experiment. Error bars indicate standard deviation derived from the photon shot noise.

indeterminate photon emission time ( $\sim 12$  ns), which can be suppressed by initializing the nitrogen nuclear spin. The spin measurement error can also be suppressed by high-fidelity manipulation with a stronger microwave.

**Polarization coincidence.** To investigate the NV-axis misalignment in more detail, we perform microwave optical double resonance (Fig. 4a). We first excite a geometric spin qubit state with a polarized microwave, followed by the  $|A_2\rangle$  excitation with a polarized light (Fig. 4b). The PSB emission from the  $|A_2\rangle$  state is maximized when the bright state against the microwave coincides with that against the light (Fig. 4c). By fitting the emission curve with a sinusoidal function, the correspondence between the microwave and light polarizations is estimated (Fig. 4d). The nonlinearity is attributed to the tilting of the NV axis. The relationship between microwave and light polarization angles can be expressed as  $\phi_{\text{MW}} = \arctan\{\alpha \tan(\phi_{\text{opt}} - \phi_{\text{NV}})\} + \phi_{\text{NV}}$ , where  $\alpha$  is the attenuation coefficient of the angle of the NV axis  $\phi_{\text{NV}}$  depending on the angle of optical polarization  $\phi_{\text{opt}}$  (see Supplementary Note 4). We estimate  $\alpha = 0.60$ ,  $\phi_{\text{NV}} = 20.1^\circ$  by fitting the experimental results shown in Fig. 4d. From the attenuation coefficient  $\alpha$ , the tilt angle of the NV axis against normal to the surface is found to be  $53.0^\circ$ , which roughly corresponds to  $54.7^\circ$  as expected from a crystal orientation of 100. The attenuation can be eliminated by using a normally oriented NV center in  $\langle 111 \rangle$ -oriented diamond. It can also be adapted by optical elements or spin manipulation to compensate for the amplitude ratio of the photon state biased by polarization distortion.

## Discussion

This demonstration differs from that in Togan et al.<sup>21</sup>, where a static magnetic field is applied to distinguish the spin up/down states. The magnetic field lifts the degeneracy to make the light polarization time-dependent although the quantum eraser technique erases the frequency information, while the degeneracy remains under a zero magnetic field in our case to keep the light polarization time-independent as well as the geometric spin qubit state. This is why the geometric spin qubit is well manipulated by a polarized microwave.

Although the present experiment did not use a single-photon microwave, it could in principle work with a one-photon process. The photon–spin entanglement measured with microwave polarization shown in Fig. 3 can be interpreted as a teleportation-based quantum state transfer of a polarized microwave photon into a polarized optical photon heralded by the detection of the ancilla state  $|0\rangle_s$  occupation. On the other hand, the polarization coincidence of a photon and microwave shown in Fig. 4 serves as a phase transfer<sup>49</sup> or conditional Bell measurement (see Supplementary Note 5). These schemes can be applied as a quantum transducer with quantum memories that interfaces superconducting or ion qubits with an optical photon via a microwave photon. Efficient transduction is expected, owing to the strong coupling of the orbital excited state with an electric field or mechanical vibration<sup>50,51</sup> in an NV center. Other possible applications include multiphoton entangled resource for quantum networks and computation<sup>52–55</sup>.

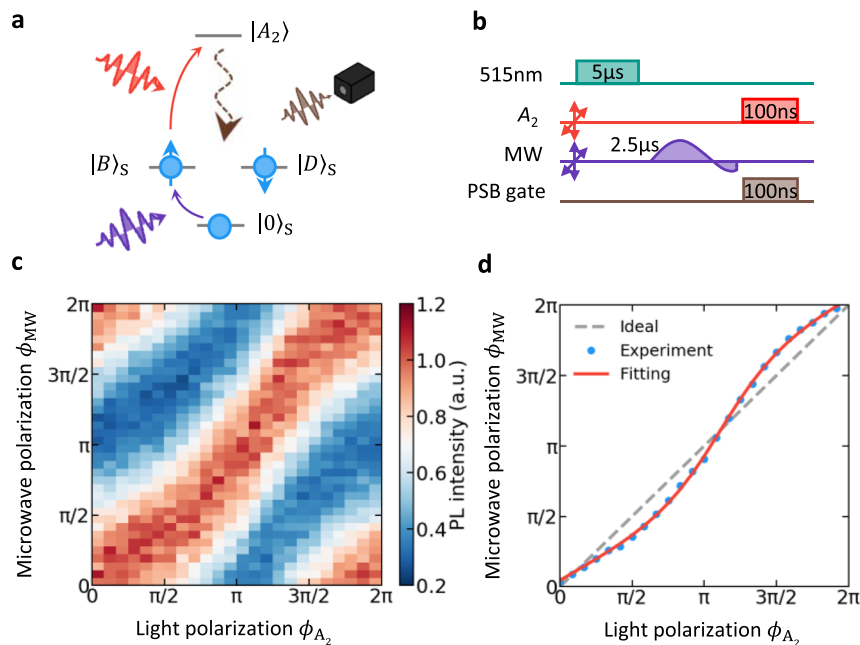


**Fig. 4** Coincidence of light and microwave polarizations. **a** Experimental schematic of microwave optical double resonance. When the bright state  $|B\rangle_s$  of the microwave and light coincide, PSB emission from  $|A_2\rangle$  is observed. **b** Experimental sequence. **c** PSB emission intensity depending on microwave and light polarizations. **d** Bright-state correspondence between microwave and light polarization obtained by fitting the data in **(c)**, where the polarization perceived by NV is distorted due to the tilt of the NV axis from the optical axis.

In conclusion, we demonstrated geometric photon–spin entanglement via spontaneous emission with the help of the spin–orbit entanglement inherent in the molecular structure of the diamond NV center under a zero magnetic field. The combination of the demonstrated scheme with the heralded quantum state transfer of a photon polarization into a nuclear spin<sup>43,44</sup> will establish a new scheme for generating heralded remote entanglement of quantum memories based on emission and absorption. The scheme is insensitive to the mode matching in time, frequency, and space, in contrast to the conventional scheme using Bell state measurement of two indistinguishable photons with a beam splitter in the middle<sup>56–60</sup>. These robustness are inherent in the physical system with complete special symmetry by excluding the unnecessary external fields. Our work paves the way for a mode-matching error-tolerant quantum network that interconnects heterogeneous quantum computers.

## Methods

We use a single naturally occurring NV center in a high-purity type IIa chemical-vapor deposition-grown diamond with a crystal orientation  $\langle 100 \rangle$  produced by element six. The diamond is cooled to 5 K to control the electron orbitals coherently. In order to achieve a zero magnetic field, the residual magnetic field including the geomagnetic field is canceled out by a three-dimensional coil. The currents of the three coils are adjusted by monitoring spin-echo coherence time, which reaches its maximum at a zero magnetic field<sup>33</sup>. Optically detected magnetic resonance measurement confirms that there are no carbon nuclear spins with hyperfine interaction above 0.1 MHz. Two orthogonal copper wires are attached to the sample surface (Fig. 1d) to apply microwaves with arbitrary polarization, which is the same configuration as ref. 40. The optical system consists of a homemade confocal microscope system (Fig. 1d), which is similar to the system used in ref. 44. The green laser is used for charge and spin initialization by nonresonant excitation, and the two red lasers are used for preparation for the  $|A_2\rangle$  state and spin measurement using the  $|E_y\rangle$  state by resonant excitation. The experimental sequences are controlled by a master homemade field-programmable gate array (FPGA) with a clock frequency of 100 MHz, which outputs digital signals to a directly modulated green laser, two acousto-optic modulators (AOM) for the red lasers, as well as the triggers for two slave arbitrary waveform generator (AWG) modulating two EOM for the red laser and two IQ mixers for the microwaves. In the spin-photon correlation experiment shown in Fig. 3, the signals from the two APD for PSB and

ZPL photons are counted and processed by the FPGA in real time in order to make the spin measurements conditioned on the ZPL photon measurement.

## Data availability

The data that support the findings of this study are available from the corresponding author upon request.

## Code availability

All codes used to produce the findings of this study are available from the corresponding author upon request.

Received: 18 March 2021; Accepted: 19 November 2021;

Published online: 15 December 2021

## References

- Kimble, H. J. The quantum internet. *Nature* **453**, 1023–1030 (2008).
- Wehner, S., Elkouss, D. & Hanson, R. Quantum internet: a vision for the road ahead. *Science* **362**, eaam9288 (2018).
- Awschalom, D. et al. Development of Quantum Interconnects (QulCs) for next-generation information technologies. *PRX Quantum* **2**, 017002 (2021).
- Kurizki, G. et al. Quantum technologies with hybrid systems. *Proc. Natl Acad. Sci. USA* **112**, 3866–3873 (2015).
- Smith, J. M., Meynell, S. A., Bleszynski Jayich, A. C. & Meijer, J. Colour centre generation in diamond for quantum technologies. *Nanophotonics* **8**, 1889–1906 (2019).
- Maze, J. R. et al. Properties of nitrogen-vacancy centers in diamond: the group theoretic approach. *N. J. Phys.* **13**, 025025 (2011).
- Doherty, M. W. et al. The nitrogen-vacancy colour centre in diamond. *Phys. Rep.* **528**, 1–45 (2013).
- Gali, Á. Ab initio theory of the nitrogen-vacancy center in diamond. *Nanophotonics* **8**, 1907–1943 (2019).
- Sukachev, D. D. et al. Silicon-vacancy spin qubit in diamond: a quantum memory exceeding 10 ms with single-shot state readout. *Phys. Rev. Lett.* **119**, 223602 (2017).
- Rose, B. C. et al. Observation of an environmentally insensitive solid-state spin defect in diamond. *Science* **361**, 60–63 (2018).
- Iwasaki, T. et al. Germanium-vacancy single color centers in diamond. *Sci. Rep.* **5**, 12882 (2015).

12. Høy Jensen, R. et al. Cavity-enhanced photon emission from a single germanium-vacancy center in a diamond membrane. *Phys. Rev. Appl.* **13**, 064016 (2020).
13. Wan, N. H. et al. Large-scale integration of artificial atoms in hybrid photonic circuits. *Nature* **583**, 226–231 (2020).
14. Iwasaki, T. et al. Tin-vacancy quantum emitters in diamond. *Phys. Rev. Lett.* **119**, 253601 (2017).
15. Trusheim, M. E. et al. Transform-limited photons from a coherent tin-vacancy spin in diamond. *Phys. Rev. Lett.* **124**, 023602 (2020).
16. Rugar, A. E. et al. Narrow-linewidth tin-vacancy centers in a diamond waveguide. *ACS Photonics* **7**, 2356–2361 (2020).
17. Awschalom, D. D., Hanson, R., Wrachtrup, J. & Zhou, B. B. Quantum technologies with optically interfaced solid-state spins. *Nat. Photonics* **12**, 516–527 (2018).
18. Bradac, C., Gao, W., Forneris, J., Trusheim, M. E. & Aharonovich, I. Quantum nanophotonics with group IV defects in diamond. *Nat. Commun.* **10**, 5625 (2019).
19. Janitz, E., Bhaskar, M. K. & Childress, L. Cavity quantum electrodynamics with color centers in diamond. *Optica* **7**, 1232 (2020).
20. Riedel, D. et al. Deterministic enhancement of coherent photon generation from a nitrogen-vacancy center in ultrapure diamond. *Phys. Rev. X* **7**, 1–8 (2017).
21. Togan, E. et al. Quantum entanglement between an optical photon and a solid-state spin qubit. *Nature* **466**, 730–734 (2010).
22. Hensen, B. et al. Loophole-free Bell inequality violation using electron spins separated by 1.3 kilometres. *Nature* **526**, 682–686 (2015).
23. Humphreys, P. C. et al. Deterministic delivery of remote entanglement on a quantum network. *Nature* **558**, 268–273 (2018).
24. Tchebotareva, A. et al. Entanglement between a diamond spin qubit and a photonic time-bin qubit at telecom wavelength. *Phys. Rev. Lett.* **123**, 063601 (2019).
25. Bhaskar, M. K. et al. Experimental demonstration of memory-enhanced quantum communication. *Nature* **580**, 60–64 (2020).
26. Waldherr, G. et al. Quantum error correction in a solid-state hybrid spin register. *Nature* **506**, 204–207 (2014).
27. Unden, T. et al. Quantum metrology enhanced by repetitive quantum error correction. *Phys. Rev. Lett.* **116**, 230502 (2016).
28. Nguyen, C. T. et al. Quantum network nodes based on diamond qubits with an efficient nanophotonic interface. *Phys. Rev. Lett.* **123**, 183602 (2019).
29. Bradley, C. E. et al. A ten-qubit solid-state spin register with quantum memory up to one minute. *Phys. Rev. X* **9**, 031045 (2019).
30. Abobeih, M. H. et al. Atomic-scale imaging of a 27-nuclear-spin cluster using a quantum sensor. *Nature* **576**, 411–415 (2019).
31. Hou, P.-Y. et al. Experimental Hamiltonian learning of an 11-qubit solid-state quantum spin register. *Chin. Phys. Lett.* **36**, 100303 (2019).
32. Kjaergaard, M. et al. Superconducting qubits: current state of play. *Annu. Rev. Condens. Matter Phys.* **11**, 369–395 (2020).
33. Sekiguchi, Y. et al. Geometric spin echo under zero field. *Nat. Commun.* **7**, 11668 (2016).
34. Dmitriev, A. K., Chen, H. Y., Fuchs, G. D. & Vershovskii, A. K. Dual-frequency spin-resonance spectroscopy of diamond nitrogen-vacancy centers in zero magnetic field. *Phys. Rev. A* **100**, 011801 (2019).
35. Kölbl, J., Kasperczyk, M., Bürgler, B., Barfuss, A. & Maletinsky, P. Determination of intrinsic effective fields and microwave polarizations by high-resolution spectroscopy of single nitrogen-vacancy center spins. *N. J. Phys.* **21**, 113039 (2019).
36. Zheng, H. et al. Zero-field magnetometry based on nitrogen-vacancy ensembles in diamond. *Phys. Rev. Appl.* **11**, 064068 (2019).
37. Kong, F. et al. KiloHertz electron paramagnetic resonance spectroscopy of single nitrogen centers at zero magnetic field. *Sci. Adv.* **6**, eaaz8244 (2020).
38. London, P., Balasubramanian, P., Naydenov, B., McGuinness, L. P. & Jelezko, F. Strong driving of a single spin using arbitrarily polarized fields. *Phys. Rev. A* **90**, 012302 (2014).
39. Herrmann, J. et al. Polarization- and frequency-tunable microwave circuit for selective excitation of nitrogen-vacancy spins in diamond. *Appl. Phys. Lett.* **109**, 183111 (2016).
40. Nagata, K., Kuramitani, K., Sekiguchi, Y. & Kosaka, H. Universal holonomic quantum gates over geometric spin qubits with polarised microwaves. *Nat. Commun.* **9**, 3227 (2018).
41. Sekiguchi, Y., Niikura, N., Kuroiwa, R., Kano, H. & Kosaka, H. Optical holonomic single quantum gates with a geometric spin under a zero field. *Nat. Photonics* **11**, 209–214 (2017).
42. Ishida, N. et al. Universal holonomic single quantum gates over a geometric spin with phase-modulated polarized light. *Opt. Lett.* **43**, 2380 (2018).
43. Yang, S. et al. High-fidelity transfer and storage of photon states in a single nuclear spin. *Nat. Photonics* **10**, 507–511 (2016).
44. Tsurumoto, K., Kuroiwa, R., Kano, H., Sekiguchi, Y. & Kosaka, H. Quantum teleportation-based state transfer of photon polarization into a carbon spin in diamond. *Commun. Phys.* **2**, 74 (2019).
45. Kosaka, H. & Niikura, N. Entangled absorption of a single photon with a single spin in diamond. *Phys. Rev. Lett.* **114**, 053603 (2015).
46. Kosaka, H. et al. Spin state tomography of optically injected electrons in a semiconductor. *Nature* **457**, 702–705 (2009).
47. Sjöqvist, E. et al. Non-adiabatic holonomic quantum computation. *New J. Phys.* **14**, 103035 (2012).
48. Khaneja, N., Reiss, T., Kehlet, C., Schulte-Herbrüggen, T. & Glaser, S. J. Optimal control of coupled spin dynamics: design of NMR pulse sequences by gradient ascent algorithms. *J. Magn. Reson.* **172**, 296–305 (2005).
49. Lekavicius, I., Golter, D. A., Oo, T. & Wang, H. Transfer of phase information between microwave and optical fields via an electron spin. *Phys. Rev. Lett.* **119**, 1–6 (2017).
50. Golter, D. A., Oo, T., Amezcua, M., Stewart, K. A. & Wang, H. Optomechanical quantum control of a nitrogen-vacancy center in diamond. *Phys. Rev. Lett.* **116**, 143602 (2016).
51. Chen, H. Y., MacQuarrie, E. R. & Fuchs, G. D. Orbital state manipulation of a diamond nitrogen-vacancy center using a mechanical resonator. *Phys. Rev. Lett.* **120**, 167401 (2018).
52. Lindner, N. H. & Rudolph, T. Proposal for pulsed on-demand sources of photonic cluster state strings. *Phys. Rev. Lett.* **103**, 1–4 (2009).
53. Buterakos, D., Barnes, E. & Economou, S. E. Deterministic generation of all-photonic quantum repeaters from solid-state emitters. *Phys. Rev. X* **7**, 1–10 (2017).
54. Pichler, H., Choi, S., Zoller, P. & Lukin, M. D. Universal photonic quantum computation via time-delayed feedback. *Proc. Natl Acad. Sci. USA* **114**, 11362–11367 (2017).
55. Russo, A., Barnes, E. & Economou, S. E. Photonic graph state generation from quantum dots and color centers for quantum communications. *Phys. Rev. B* **98**, 1–12 (2018).
56. Moehring, D. L. et al. Entanglement of single-atom quantum bits at a distance. *Nature* **449**, 68–71 (2007).
57. Ritter, S. et al. An elementary quantum network of single atoms in optical cavities. *Nature* **484**, 195–200 (2012).
58. Hofmann, J. et al. Heralded entanglement between widely separated atoms. *Science* **337**, 72–75 (2012).
59. Bernien, H. et al. Heralded entanglement between solid-state qubits separated by three metres. *Nature* **497**, 86–90 (2013).
60. Delteil, A. et al. Generation of heralded entanglement between distant hole spins. *Nat. Phys.* **12**, 218–223 (2016).

## Acknowledgements

We thank Hiromitsu Kato, Toshiharu Makino, Tokuyuki Teraji, Yuichiro Matsuzaki, Kae Nemoto, Norikazu Mizuochi, Fedor Jelezko, and Joerg Wrachtrup for their discussions and experimental help. This work was supported by the Japan Society for the Promotion of Science (JSPS) Grants-in-Aid for Scientific Research (20H05661, 20K20441); by a Japan Science and Technology Agency (JST) CREST (JPMJCR1773); and by a JST Moonshot R&D (JPMJMS2062). We also acknowledge the Ministry of Internal Affairs and Communications (MIC), Research and development for the construction of a global quantum cryptography network (JPMI00316).

## Author contributions

Y.S., Y.Y., and K.T. carried out the experiment. Y.K. and R.R. supported the experiment. Y.S. analyzed the data. Y.S. and H.K. wrote the manuscript. H.K. supervised the project. All authors discussed the results and commented on the manuscript.

## Competing interests

The authors declare no competing interests.

## Additional information

**Supplementary information** The online version contains supplementary material available at <https://doi.org/10.1038/s42005-021-00767-1>.

**Correspondence** and requests for materials should be addressed to Hideo Kosaka.

**Peer review information** *Communications Physics* thanks M. V. Gurudev Dutt and the other, anonymous, reviewer(s) for their contribution to the peer review of this work. This article has been peer reviewed as part of Springer Nature's [Guided Open Access](#) initiative.

**Reprints and permission information** is available at <http://www.nature.com/reprints>

**Publisher's note** Springer Nature remains neutral with regard to jurisdictional claims in published maps and institutional affiliations.



**Open Access** This article is licensed under a Creative Commons Attribution 4.0 International License, which permits use, sharing, adaptation, distribution and reproduction in any medium or format, as long as you give appropriate credit to the original author(s) and the source, provide a link to the Creative Commons license, and indicate if changes were made. The images or other third party material in this article are included in the article's Creative Commons license, unless indicated otherwise in a credit line to the material. If material is not included in the article's Creative Commons license and your intended use is not permitted by statutory regulation or exceeds the permitted use, you will need to obtain permission directly from the copyright holder. To view a copy of this license, visit <http://creativecommons.org/licenses/by/4.0/>.

© The Author(s) 2021